Effects of Alkoxy Chain Length in Alkoxy-Substituted Dihydronaphthyl-Based [60]Fullerene Bisadduct Acceptors on Their Photovoltaic Properties

Xiangyue Meng,[†,‡] Qi Xu,[§] Wenqing Zhang,[§] Zhan'ao Tan,*[,§] Yongfang Li,[∇] Zhuxia Zhang,[†] Li Jiang,[†] Chunying Shu,[†] and Chunru Wang*[,†]

[†]Key Laboratory of Molecular Nanostructure and Nanotechnology, Beijing National Laboratory for Molecular Sciences, Institute of Chemistry, Chinese Academy of Sciences, Beijing 100190, China

[‡]Graduate University of Chinese Academy of Sciences, Beijing 100049, China

[§]State Key Laboratory of Alternate Electrical Power System with Renewable Energy Sources, The New and Renewable Energy of Beijing Key Laboratory, North China Electric Power University, Beijing 102206, China

[∇]Key Laboratory of Organic Solids, Institute of Chemistry, Chinese Academy of Sciences, Beijing 100190, China

Ⓢ Supporting Information

ABSTRACT: A series of alkoxy-substituted dihydronaphthyl-based [60]fullerene bisadduct derivatives (Cn-NCBA, n = 1–6), with the alkoxy chain length from 1 to 6 carbon atoms, were synthesized as acceptors for polymer solar cells (PSCs), for the purpose of systematically investigating the effects of fullerene derivative structures on the photovoltaic properties of PSCs. Although the absorption spectra and electrochemical properties of Cn-NCBA are almost the same, the PSCs based on P3HT:Cn-NCBA showed different photovoltaic properties. The device based on the P3HT:C3-NCBA blend demon-

strated the highest power-conversion efficiency (PCE) of ca. 4.1%, while those with shorter or longer alkoxy-substituted dihydronaphthyl-based [60]fullerene bisadduct derivatives showed relatively lower PCE values. C5-NCBA and C6-NCBA with longer alkoxy chain length showed relatively low electron mobilities, leading to relatively poor photovoltaic performance. More importantly, we found that the alkoxy chain length changes the hydrophobicity of Cn-NCBA and, thus, the interfacial interaction and miscibility with P3HT, which were analyzed by interfacial tension and atomic force microscopy (AFM) measurements. The hydrophobicity of Cn-NCBA increased as the alkoxy chain length increased. A distinct phase separation for the P3HT:C1-NCBA blend film due to the large interfacial tension and poor miscibility between P3HT and C1-NCBA could be one reason for the low PCE value of the C1-NCBA-based devices. C3-NCBA may provide the most appropriate combination of electron mobility and miscibility with P3HT to achieve optimal photovoltaic properties. The current study provides the molecular structure–device performance relationship, especially with respect to the alkoxy chain length of Cn-NCBA and their interfacial interactions with P3HT, and suggests a design rule for high-performance fullerene bisadduct acceptors for PSC applications.

KEYWORDS: polymer solar cell, electron acceptor, bisadduct fullerene, chain length, miscibility, electron mobility
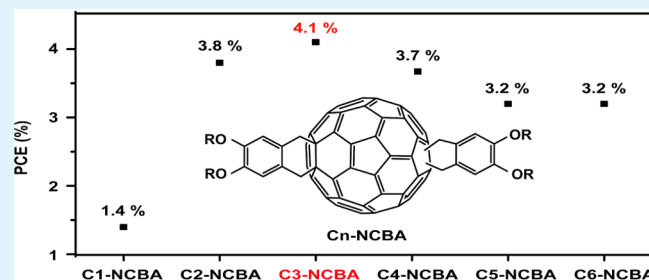
■ INTRODUCTION

Polymer solar cells (PSCs) have emerged as a promising source of alternative energies, because of the advantages of low cost, light weight, and flexibility.[1−3] To maximize the donor–acceptor heterojunction interfacial area for efficient exciton dissociation, mainstream PSC devices adopt the concept of a bulk heterojunction (BHJ), where a photoactive layer contains a *p*-type conjugated polymer donor and an *n*-type fullerene derivative acceptor to form an interpenetrating network.[4] In order to improve power-conversion efficiency (PCE) of the PSCs, great efforts have been devoted to explore novel low-bandgap conjugated-polymer donor[5−7] and the matching fullerene derivative acceptor materials,[8,9] in which the poly(3-hexylthiophene) (P3HT) and [6,6]-phenyl-C_{61}-butyric acid

methyl ester (PCBM)[10] are the most representative donor and acceptor materials, respectively.

However, one of the main bottlenecks for the P3HT:PCBM-based PSCs is the low open-circuit voltage (V_{oc}) value of ca. 0.6 V, which results in a limited PCE of only ca. 4%.[11,12] It is well-established that the V_{oc} value is related to the difference between the highest occupied molecular orbital (HOMO) energy level of the donor and the lowest unoccupied molecular orbital (LUMO) energy level of the acceptor,[13] so an upshift of the LUMO energy level of the fullerene acceptor is preferred

for increasing the V_{oc} values.[14] Recently, a series of high V_{oc} P3HT-based PSCs have been obtained using fullerene bisadduct derivatives with higher LUMO energy level.[15−20] For example, Lenes et al.[21] synthesized [60]PCBM bisadduct (bisPCBM) with LUMO energy level ca. 0.1 eV higher than that of PCBM. The V_{oc} and PCE values of the PSC based on P3HT:bisPCBM reached 0.73 V and 4.5%, respectively, whereas the P3HT:PCBM-based solar cell has V_{oc} and PCE values of only 0.58 V and 3.4%, respectively, under the same conditions. The relative higher LUMO energy level of bisPCBM, compared to PCBM, is induced by the reduced π-conjugation and electron delocalization of the fullerene sphere after the second addend is added.[22] Recently, PSCs with fullerene bisadduct derivatives other than PCBM have attracted extensive attention, because of their relative high PCEs. Especially, a remarkable bisadduct fullerene derivative, ICBA (indene-C_{60} bisadduct), has been reported.[23] The LUMO energy level of ICBA is 0.17 eV higher than that of PCBM. As a consequence, the optimized PSC with the P3HT:ICBA as the photoactive layer exhibited a high V_{oc} value of 0.84 V and the PCE value was as high as 6.48%.[24] Recently, Hsu et al.[25] reported the di(4-methylphenyl)methano-C_{60} bisadduct (DMPCBA), whose LUMO energy level is ca. 0.1 eV higher than PCBM, and the PSC based on the P3HT:DMPCBA blend exhibited a high V_{oc} value of ca. 0.87 V, as well as a high PCE value of ca. 5.2%. Very recently, we reported a dihydronaphthyl-based [60]fullerene bisadduct derivative ($NC_{60}BA$).[26] The PSC based on the P3HT:NC_{60}BA blend not only had a high V_{oc} value of ca. 0.82 V and a high PCE value of ca. 5.37%, but it also exhibited high thermal stability, which was due to the amorphous nature of NC_{60}BA, which effectively suppressed the thermal-driven crystallization. For further improving the visible absorption of the fullerene derivative, the dihydronaphthyl-based [70]fullerene bisadduct derivative ($NC_{70}BA$) was synthesized and explored as an acceptor in PSCs.[27] The NC_{70}BA has a LUMO energy level that is 0.2 eV higher than PCBM and displays increased and broad absorption in the visible region. Consequently, the PSC based on P3HT:NC_{70}BA showed a high V_{oc} value (0.83 V) and a high PCE value (5.95%). Undoubtedly, fullerene bisadduct derivatives[28,29] have emerged as efficient acceptors for PSC applications.

Both NC_{60}BA-based and NC_{70}BA-based PSC devices showed excellent photovoltaic properties and high thermal stability when blended with P3HT, indicating that this family of fullerene derivatives has the potential to be applied in practical PSCs. To further explore this family of fullerene derivatives, a series of alkoxy-substituted dihydronaphthyl-based [60]-fullerene bisadduct derivatives (Cn-NCBA, $n = 1−6$) were designed, by changing the alkoxy chain length from 1 to 6 carbon atoms, respectively, and the effects of alkoxy chain length of Cn-NCBA on the physical properties and photovoltaic properties were investigated. Cn-NCBA ($n = 1−6$) demonstrate almost the same light absorption and electrochemical properties. However, the PSCs based on P3HT as a donor and Cn-NCBA as acceptors showed different photovoltaic properties. The PSCs with C3-NCBA as the acceptor displayed highest photovoltaic performance with a PCE value of 4.1% among the series of Cn-NCBA, while those with shorter or longer alkoxy-substituted dihydronaphthyl-based [60]fullerene bisadduct derivatives showed relatively lower PCE. C5-NCBA and C6-NCBA with longer alkoxy chain length showed relatively low electron mobilities, leading to relatively poor photovoltaic performance. We also found that the alkoxy

chain length changes the hydrophobicity of Cn-NCBA and thus the interfacial interaction and miscibility with P3HT. Direct evidence of changes in the interfacial interaction was provided by measurements of the surface tension of Cn-NCBA and their corresponding interfacial tensions with P3HT. The results were supported by atomic force microscopy (AFM) measurements. The hydrophobicity of Cn-NCBA and miscibility with P3HT increased with the increase of alkoxy chain length. A distinct phase separation for the P3HT:C1-NCBA blend film due to the large interfacial tension and poor miscibility with P3HT could be one reason for the low PCE of the C1-NCBA-based devices. C3-NCBA may provide the most appropriate combination of electron mobility and miscibility with P3HT to achieve optimal photovoltaic properties. The alkoxy chain length has been shown to have a pronounced effect on the electron mobility and morphology, and, thus, device performance.

■ EXPERIMENTAL SECTION

Materials and Characterization. All chemicals were purchased from commercial sources and used without further purificaton, and the solvents were purified and freshly distilled prior to use according to literature procedures. 1,2-Dimethoxybenzene (**1a**) was purchased from Alfa-Aesar, and 1,2-dialkoxybenzene (**1b−1f**) were prepared according to previously reported procedures.[30] P3HT (4002-E) was purchased from Rieke Metals, Inc. ^{1}H NMR and ^{13}C NMR spectra were recorded on Bruker DMX-400 and Bruker DMX-600 spectrometer. Absorption spectra were taken on a Hitachi U-3010 UV−vis spectrophotometer. The electrochemical cyclic voltammetry was conducted on a Zahner IM6e Electrochemical Workstation. A Pt disk was taken as the working electrode, Pt wire as the counter electrode, and Ag/Ag$^+$ electrode (0.01 M AgNO$_3$, 0.09 M NBu$_4$PF$_6$ in acetonitrile) as the reference electrode. A mixed solution of o-dichlorobenzene:acetonitrile (v:v = 5:1) with 0.1 M tetrabutylammonium hexafluorophosphate (NBu$_4$PF$_6$) was used as electrolyte, and the scan rate was fixed at 100 mV s$^{−1}$. High-performance liquid chromatography (HPLC) analysis was performed on LC908-C60 (Jai Co., Ltd.) with a Cosmosil Buckyprep column (∅20 mm × 250 mm, Nacalai USA), using toluene as an eluent. AFM images under tapping mode were taken on a Veeco NanoScope IIIa SPM (DI, USA). Contact angle (CA) was measured on an OCA20 contact angle system (Data-Physics, Germany). Solutions of P3HT, PCBM, and NCBA in o-dichlorobenzene (10 mg mL$^{−1}$) were prepared and then passed through a 0.2-μm PTFE syringe filter. Each solution was spin-cast onto a glass substrate at 800 rpm for 60 s. Two microliters (2 μL) of water or glycerol was dipped onto the as-prepared film. The CA value is automatically given by the system. Each sample was measured five times and an average value of CA was given.

1,2-Bis(bromomethyl)-4,5-dimethoxybenzene (2a). To a mixture of 1,2-dimethoxybenzene (56.5 mmol, 1 equiv) and paraformaldehyde (141.3 mmol, 2.5 equiv) dissolved in CH$_2$Cl$_2$ (30 mL) were added hydrogen bromide (33% (w/w) in AcOH, 169.5 mmol, 3 equiv) and AcOH (70 mL). The mixture was stirred at room temperature under an argon atmosphere for 24 h. The white precipitate formed during the period was separated from the solution by filtration, washed with AcOH, and dried under vacuum to give compound **2a** as a white powder. Yield: 72%. ^{1}H NMR (400 MHz, CDCl$_3$): δ (ppm) 6.84 (s, 2H), 4.63 (s, 4H), 3.90 (s, 6H).

1,2-Bis(bromomethyl)-4,5-diethoxybenzene (2b). Prepared as described for compound **2a**. Yield: 75%. ^{1}H NMR (400 MHz, CDCl$_3$): δ (ppm) 6.84 (s, 2H), 4.62 (s, 4H), 4.10 (m, 4H), 1.45 (t, 6H).

1,2-Bis(bromomethyl)-4,5-dipropoxybenzene (2c). Prepared as described for compound **2a**. Yield: 76%. ^{1}H NMR (400 MHz, CDCl$_3$): δ (ppm) 6.84 (s, 2H), 4.62 (s, 4H), 3.97 (t, 4H), 1.80−1.90 (m, 8H), 1.06 (t, 6H).

1,2-Bis(bromomethyl)-4,5-dibutoxybenzene (2d). Prepared as described for compound **2a**. Yield: 64%. ^{1}H NMR (400 MHz,

CDCl$_3$): δ (ppm) 6.84 (s, 2H), 4.62 (s, 4H), 4.00 (t, 4H), 1.80 (m, 4H), 1.45−1.54 (m, 4H), 0.96 (t, 6H).

1,2-Bis(bromomethyl)-4,5-bis(pentyloxy)benzene (2e). This compound was prepared as described for compound **2a**. Yield: 67%. ^{1}H NMR (400 MHz, CDCl$_3$): δ (ppm) 6.83 (s, 2H), 4.62 (s, 4H), 4.00 (t, 4H), 1.82 (m, 4H), 1.35−1.49 (m, 8H), 0.93 (t, 6H).

1,2-Bis(bromomethyl)-4,5-bis(hexyloxy)benzene (2f). This compound was prepared as described for compound **2a**. Yield: 65%. ^{1}H NMR (400 MHz, CDCl$_3$): δ (ppm) 6.84 (s, 2H), 4.62 (s, 4H), 3.99 (t, 4H), 1.81 (m, 4H), 1.46 (m, 4H), 1.31−1.35 (m, 8H), 0.91 (t, 6H).

General Procedure for the Synthesis of Sultines (3a−3f). To a solution of the corresponding bis(bromomethyl) derivative **2a−2f** (1 equiv) in anhydrous DMF were added sodium hydroxymethanesulfinate (rongalite, 3 equiv) and tetrabutylammonium bromide (TBAB, 0.3 equiv) under argon. The mixture was stirred at 0 °C under an argon atmosphere for 4 h, then water was added and the mixture was extracted with CH$_2$Cl$_2$. The organic extracts were dried over NaSO$_4$, and the solvent was evaporated at 30 °C to give a colorless oil. The crude product was subjected to the next reaction without further purification.

C1-NCBA. To a solution of C$_{60}$ (0.302 mmol, 1 equiv) in toluene (250 mL) was added the sultine **3a** (0.906 mmol, 3 equiv). The mixture was heated at 100 °C under an argon atmosphere for 15 h. After cooling, water was added and the mixture was extracted with toluene. The organic extracts were dried over NaSO$_4$, and concentrated under reduced pressure. The crude product was first purified by silica gel column chromatography, and further purification by preparative HPLC equipped with a Buckyprep column, using toluene as an eluent, afforded brown powder. Yield: 36%. ^{1}H NMR (400 MHz, CDCl$_3$): δ (ppm) 6.93−7.41 (m, 4H), 3.75−4.92 (m, 20H). ^{13}C NMR (600 MHz, CDCl$_3$): δ (ppm) 148.51, 148.19, 146.75, 145.59, 145.44, 145.04, 144.82, 143.78, 141.59, 141.32, 130.06, 111.50, 111.26, 77.25, 77.03, 76.82, 67.99, 65.33, 65.10, 65.02, 64.70, 64.60, 56.21, 45.05, 44.80. MALDI-TOF MS: calcd. 1048.17; found 1048.19.

C2-NCBA. Prepared as described for compound C1-NCBA. Yield: 45%. ^{1}H NMR (400 MHz, CDCl$_3$): δ (ppm) 6.92−7.38 (m, 4H), 3.55−4.87 (m, 16H), 1.46−1.56 (m, 12H). ^{13}C NMR (600 MHz, CDCl$_3$): δ (ppm) 154.99, 149.13, 148.60, 148.33, 148.11, 146.67, 146.43, 146.24, 145.91, 145.52, 145.37, 145.14, 144.98, 144.74, 144.68, 144.51, 143.69, 142.42, 142.21, 141.50, 141.23, 130.19, 113.60, 113.36, 77.23, 77.02, 76.80, 67.94, 65.30, 65.00, 64.88, 64.73, 64.66, 64.57, 45.11, 44.94, 44.70, 44.53, 44.34, 43.37. MALDI-TOF MS: calcd. 1104.23; found 1104.61.

C3-NCBA. Prepared as described for compound C1-NCBA. Yield: 41%. ^{1}H NMR (400 MHz, CDCl$_3$): δ (ppm) 6.82−7.33 (m, 4H), 3.61−4.90 (m, 16H), 1.88−1.99 (m, 8H), 1.04−1.17 (m, 12H). ^{13}C NMR (600 MHz, CDCl$_3$): δ (ppm) 146.73, 146.31, 145.97, 145.58, 145.42, 145.20, 145.05, 144.80, 144.74, 144.58, 143.75, 142.49, 141.56, 141.29, 130.33, 114.45, 114.14, 113.88, 77.25, 77.04, 76.83, 71.16, 65.35, 65.12, 65.05, 64.85, 64.78, 64.71, 64.61, 45.00, 44.87, 44.77, 44.41. MALDI-TOF MS: calcd. 1160.29; found 1160.57.

C4-NCBA. Prepared as described for compound C1-NCBA. Yield: 35%. ^{1}H NMR (400 MHz, CDCl$_3$): δ (ppm) 6.93−7.41 (m, 4H), 3.73−4.89 (m, 16H), 1.85−1.88 (m, 8H), 1.55−1.62 (m, 8H), 0.97−1.07 (m, 12H). ^{13}C NMR (600 MHz, CDCl$_3$): δ (ppm) 148.83, 148.64, 148.18, 145.59, 145.43, 144.80, 143.75, 141.56, 130.38, 114.18, 113.93, 77.25, 77.04, 76.83, 69.42, 67.99, 65.35, 65.13, 65.05, 64.78, 64.72, 64.62, 44.76. MALDI-TOF MS: calcd. 1216.36; found 1216.39.

C5-NCBA. Prepared as described for compound C1-NCBA. Yield: 42%. ^{1}H NMR (400 MHz, CDCl$_3$): δ (ppm) 6.92−7.39 (m, 4H), 3.55−4.88 (m, 16H), 1.85−1.89 (m, 8H), 1.43−1.57 (m, 16H), 0.92−0.98 (m, 12H). ^{13}C NMR (600 MHz, CDCl$_3$): δ (ppm) 155.57, 155.03, 149.11, 148.76, 148.60, 148.11, 147.26, 146.66, 146.43, 146.23, 145.90, 145.52, 145.36, 145.14, 144.99, 144.74, 144.66, 144.51, 143.69, 142.43, 142.21, 141.50, 141.21, 130.25, 114.05, 113.80, 77.23, 77.02, 76.81, 69.62, 65.29, 64.99, 64.72, 64.65, 64.55, 45.11, 44.93, 44.69, 44.53, 44.33, 43.39. MALDI-TOF MS: calcd. 1272.42; found 1272.44.

C6-NCBA. Prepared as described for compound C1-NCBA. Yield: 46%. ^{1}H NMR (400 MHz, CDCl$_3$): δ (ppm) 6.84−7.32 (m, 4H), 3.62−4.80 (m, 16H), 1.76−1.81 (m, 8H), 1.43−1.45 (m, 8H), 1.27−1.31 (m, 16H), 0.82−0.85 (m, 12H). ^{13}C NMR (600 MHz, CDCl$_3$): δ (ppm) 148.61, 148.18, 146.73, 145.58, 145.42, 145.20, 145.05, 144.80, 144.73, 144.57, 143.75, 141.56, 141.29, 130.28, 114.11, 113.88, 77.28, 77.06, 76.85, 69.70, 68.00, 65.36, 65.13, 65.05, 64.79, 64.71, 64.62, 44.76. MALDI-TOF MS: calcd. 1328.48; found 1328.37.

Device Fabrication and Characterization. The PSCs were fabricated in the configuration of the traditional sandwich structure ITO/PEDOT:PSS/BHJ/Ca/Al. The ITO glass was cleaned by sequential ultrasonic treatment in detergent, deionized water, acetone, and isopropanol, and then treated in an ultraviolet−ozone chamber (Ultraviolet Ozone Cleaner, Jelight Company, USA) for 20 min. Then PEDOT:PSS (poly(3,4-ethylene dioxythiophene):poly(styrene sulfonate)) (Baytron PVPAI 4083, Germany) was filtered through a 0.45-μm filter and spin-coated at 4000 rpm for 60 s on the ITO electrode. Subsequently, the PEDOT:PSS film was baked at 150 °C for 20 min in the air. The blend solution of P3HT and different fullerene derivative acceptors in dichlorobenzene (DCB) (the total concentration is 34 mg mL^{-1}, and the P3HT:acceptor weight ratio is 1:1.2) was spin-coated on top of the PEDOT:PSS layer. The blend films were then put into glass Petri dishes while still wet to undergo solvent annealing process. The thickness of the photoactive layer was estimated by a surface profiler in the range of 180−220 nm. The device was annealed at 120 °C for 10 min. A bilayer cathode consisted of calcium (20 nm) capped with aluminum (100 nm) was thermal-evaporated under a shadow mask in a base pressure of ca. 10^{-4} Pa. The device active area of the PSCs is ca. 4 mm^2. The J−V measurement of the devices was conducted on a computer-controlled Keithley 236 source measure unit. Device characterization was done in glovebox under simulated AM1.5G irradiation (100 mW cm^{-2}), using a xenon-lamp-based solar simulator (from Newport Co., Ltd.). The EQE measurements of the PSCs were performed using a lock-in amplifier (Stanford Research Systems, model SR830 DSP) coupled with a Model WDG3 monochromator and a 500-W xenon lamp. The light intensity at each wavelength was calibrated with a standard single-crystal Si photovoltaic cell. For the electron-only devices, the electron mobilities of P3HT:Cn-NCBA and P3HT:PCBM blend films were measured under the optimized device condition. An aluminum film (50 nm) was thermally evaporated onto a glass slide. The P3HT:fullerene derivative solutions were spin-coated onto the aluminum film/glass substrate. Then, an aluminum (100 nm) electrode was thermally evaporated onto the blend film through a shadow mask. The measurement of electron mobilities was conducted in darkness by the space-charge limited current (SLC) method on a computer-controlled Keithley 236 source measure unit.

RESULTS AND DISCUSSION

Synthesis. The synthetic route to Cn-NCBA (n = 1−6) is shown in Scheme 1. First, the reaction of 1,2-dialkyloxybenzene (**1a−1f**) with a solution of HBr in acetic acid and paraformaldehyde at room temperature led to **2a−2f**.[31,32] Then, sultines **3a−3f** were synthesized from the respective 1,2-

Scheme 1. Synthetic Route to Cn-NCBA (n = 1−6)

5968

dx.doi.org/10.1021/am301629d | ACS Appl. Mater. Interfaces 2012, 4, 5966−5973
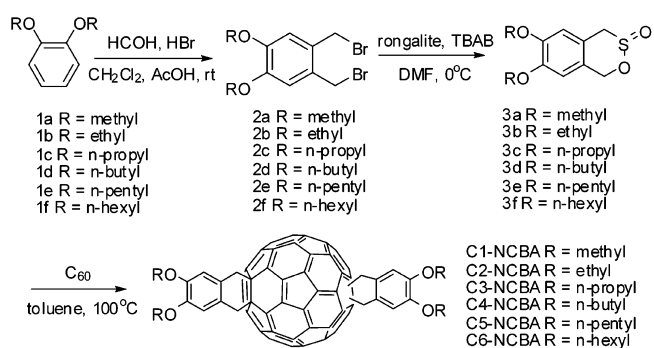
bis(bromomethyl)-4,5-dialkoxybenzene via reaction with sodium hydroxymethanesulfinate ("rongalite") in anhydrous N,N-dimethylformamide (DMF) with a catalytic amount of tetrabutylammonium bromide (TBAB) at 0 °C.[33] Finally, the sultines **3a–3f** reacted with C_{60} in toluene by extrusion of SO_2 and in situ generation of the respective substituted o-quinodimethanes, which were readily trapped by C_{60} acting as the dienophile.[34] The crude products were purified by silica gel column chromatography and HPLC in succession. The molecular structure of Cn-NCBA (n = 1−6) were confirmed by MALDI-TOF mass spectrometry, ^{1}H NMR spectrometry, and ^{13}C NMR spectrometry.

Optical Properties. The UV−vis absorption spectra of the fullerene derivatives in THF are shown in Figure 1. The
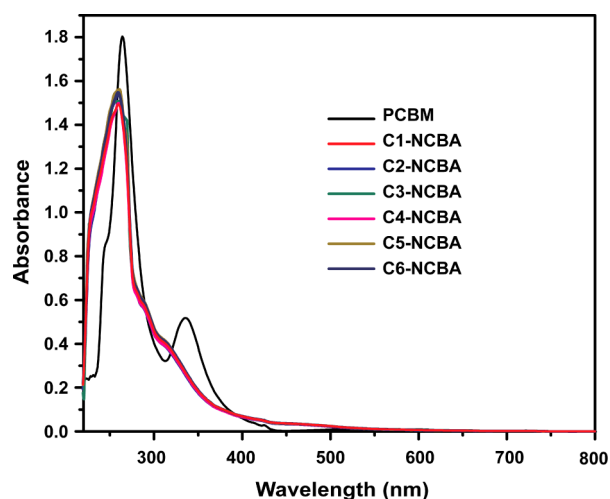

Figure 1. Absorption spectra of Cn-NCBA (n = 1−6) and PCBM in THF solutions (10^{-5} mol L^{-1}).

absorption spectra of Cn-NCBA (n = 1−6) derivatives are quite similar, indicating that the alkoxy chain length in the alkoxy-substituted dihydronaphthyl-based [60]fullerene bisadduct derivatives has little effect on the absorption spectra.[35]

Electrochemical Properties. The electrochemical properties of the fullerene derivatives were investigated by cyclic voltammetry. As shown in Figure 2, the cyclic voltammograms of Cn-NCBA exhibit three similar quasi-reversible reduction waves in the negative potential range from 0 to −2.5 V vs Ag/Ag+. It can be seen that the first (E_1), second (E_2), and third (E_3) reduction potentials, as well as the onset reduction potentials (E_{red}^{on}) of Cn-NCBA negatively shift, compared to PCBM. In fact, the LUMO energy levels of the fullerene derivatives can be estimated from E_{red}^{on} according to the following equation:

$$E_{LUMO}\ (eV) = -e(E_{red}^{on} + 4.71)$$

Cn-NCBA compounds have almost the same LUMO energy levels: ca. −3.74 eV (see the Supporting Information), which is ca. 0.18 eV higher than that of PCBM (ca. −3.92 eV). It should be mentioned that the LUMO energy level of $NC_{60}BA$ in our previous study is ca. −3.76 eV,[26] which is 0.02 eV lower than that of Cn-NCBA. The reason why Cn-NCBA has a slightly higher LUMO energy level than $NC_{60}BA$ is that alkoxy is, in fact, an electron-donating group,[36,37] and the high LUMO energy level of Cn-NCBA should be preferable to improve V_{oc}.
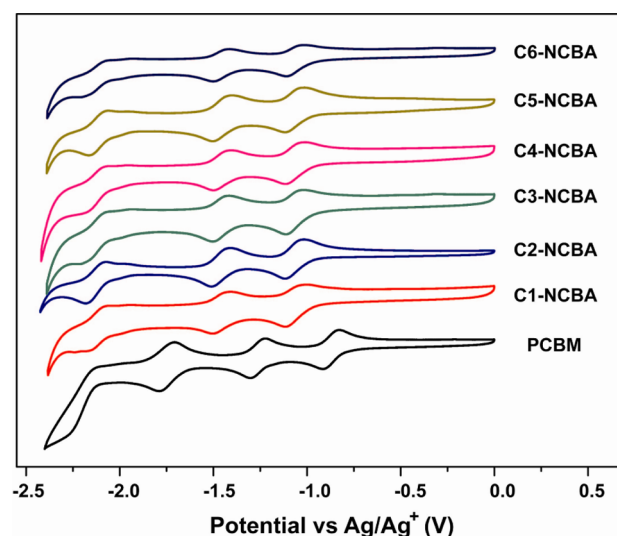
Figure 2. Cyclic voltammograms of Cn-NCBA (n = 1−6) and PCBM in o-dichlorobenzene:acetonitrile (v:v = 5:1) with 0.1 M NBu_4PF_6 at 100 mV s^{-1}.

Photovoltaic Properties. To investigate the effect of alkoxy chain length in the alkoxy-substituted dihydronaphthyl-based [60]fullerene bisadduct derivatives on their photovoltaic properties, BHJ solar cells based on the ITO/PEDOT:PSS/P3HT:acceptor/Ca/Al configuration were fabricated and characterized under simulated AM 1.5 G illumination (100 mW cm^{-2}). The concentration for all blend solutions in o-DCB was optimized to be 34 mg/mL. The donor−acceptor weight ratio and the annealing temperature for the devices were optimized to be 1:1.2 and 120 °C, respectively (see the Supporting Information). The current density−voltage curves of the devices separately using Cn-NCBA and PCBM as the acceptor are shown in Figure 3, and the resulting V_{oc}, short-circuit current (J_{sc}), fill factor (FF), and PCE of the devices are summarized in Table 1.

Obviously, Cn-NCBA-based devices showed higher V_{oc} values than the control PCBM-based solar cell, because of the higher LUMO energy levels of Cn-NCBA. It can be seen from Table 1 that the P3HT:C3-NCBA device afforded a
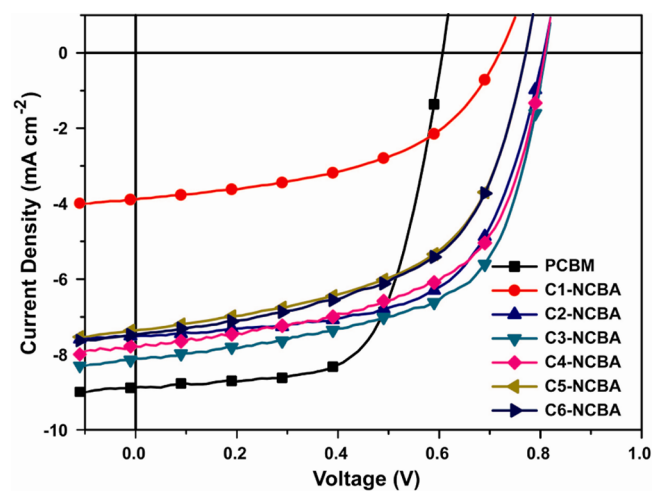
Figure 3. Current density−voltage curves of the PSCs based on P3HT:Cn-NCBA and P3HT:PCBM blends.

5969

dx.doi.org/10.1021/am301629d | ACS Appl. Mater. Interfaces 2012, 4, 5966−5973

Table 1. Device Characteristics of P3HT-Based Solar Cells

	open-circuit voltage, V_{oc} (V)	short-circuit current, J_{sc} (mA/cm^2)	fill factor, FF	power-conversion efficiency, PCE (%)	electron mobility (cm^2 V^{-1} s^{-1})	RMS roughness (nm)
C1-NCBA	0.72	3.85	0.50	1.4	3.7×10^{-5}	33.6
C2-NCBA	0.81	7.50	0.62	3.8	7.7×10^{-5}	16.5
C3-NCBA	0.81	8.12	0.62	4.1	8.6×10^{-5}	12.1
C4-NCBA	0.81	7.79	0.58	3.7	4.1×10^{-5}	13.1
C5-NCBA	0.78	7.28	0.56	3.2	9.5×10^{-6}	12.7
C6-NCBA	0.77	7.39	0.57	3.2	9.2×10^{-6}	13.3
PCBM	0.62	9.19	0.59	3.4	1.7×10^{-4}	11.8

highest PCE of 4.1%, the PSCs based on P3HT:C2-NCBA and P3HT:C4-NCBA blends demonstrated slightly lower PCE values of 3.8% and 3.7%, respectively, whereas the P3HT:C5-NCBA, P3HT:C6-NCBA, and P3HT:C1-NCBA solar cells separately showed much lower PCEs of ca. 3.2%, 3.2%, and 1.4%, respectively. C2-NCBA, C3-NCBA, and C4-NCBA exhibited superior photovoltaic performance, compared to PCBM-based devices under the same conditions, indicating that they are promising acceptor materials for PSC applications. Since all of the fullerene derivatives exhibit similar light absorption and electrochemical properties, the photovoltaic performance difference of the P3HT:Cn-NCBA devices may be ascribed to their structural changes, which lead to different electron mobility and film morphology, etc.

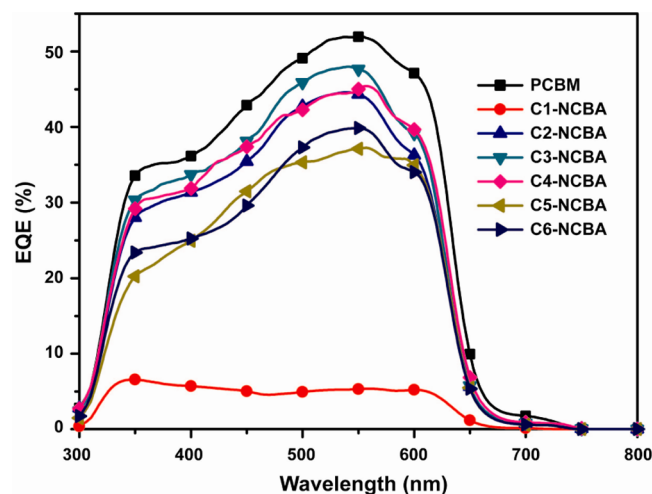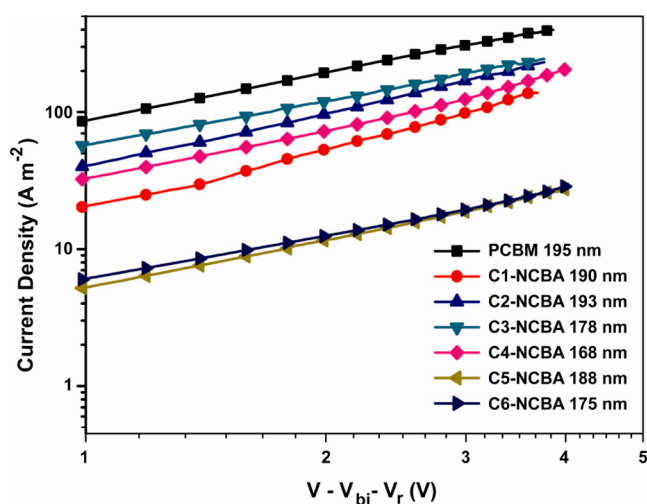External quantum efficiency (EQE) plots of the PSCs based on P3HT:Cn-NCBA and P3HT:PCBM are shown in Figure 4.

Figure 5. J−V characteristics of electron-only devices based on P3HT:Cn-NCBA and P3HT:PCBM blends under the optimized device condition. The numbers shown in plots are the film thickness of the samples.

Figure 4. External quantum efficiency of the PSCs based on P3HT:Cn-NCBA and P3HT:PCBM blends.

Except for the C1-NCBA-based device, which showed obvious low EQE, all the devices based on Cn-NCBA (n = 2, 3, 4, 5, 6) showed high EQE values, suggesting efficient photon-electron conversion processes.

Electron Mobility. To determine the effect of alkoxy chain length on electron mobility, electron mobilities of P3HT:Cn-NCBA and P3HT:PCBM blend films were measured by the space-charge limited current (SCLC) method with the electron-only devices (Al/P3HT:acceptor/Al). J−V curves of the electron-only devices are described in Figure 5, with relevant values of electron mobilities summarized in Table 1.

The electron mobilities obtained for the P3HT:C2-NCBA, P3HT:C3-NCBA, and P3HT:C4-NCBA blend films are 7.7×10^{-5}, 8.6×10^{-5}, and 4.1×10^{-5} cm^2 V^{-1} s^{-1}, respectively. The

relatively high carrier mobility would contribute to the high photocurrents and fill factors in optimized BHJ devices. The electron mobility of 1.7×10^{-4} cm^2 V^{-1} s^{-1} for P3HT:PCBM is close to that reported in the literature,[38] confirming the validity of the measurements. Previous study has theoretically predicted that the electron mobility of the fullerene derivative decreases as the length of the aliphatic side chain increases, because the aliphatic side chain can disrupt the optimal packing of fullerene and block electron transport.[39] The as-prepared C5-NCBA and C6-NCBA with longer alkoxy chain length showed relatively low electron mobilities (on the order of 10^{-6} cm^2 V^{-1} s^{-1}), which should account for the low PCE of the P3HT:C5-NCBA and P3HT:C6-NCBA devices.

Morphology. An atomic force microscopy (AFM) technique in tapping mode was employed to measure the nanoscale morphologies of the P3HT:Cn-NCBA and P3HT:PCBM blend films, as shown in Figures 6 (height image) and 7 (phase image). In order to quantitatively compare the morphology of different films, values of the root-mean-square (RMS) surface roughnesses of the P3HT:Cn-NCBA and P3HT:PCBM blend films are summarized in Table 1.

The RMS roughnesses of the P3HT:C2-NCBA, P3HT:C3-NCBA, P3HT:C4-NCBA, P3HT:C5-NCBA, and P3HT:C6-NCBA blend films are 16.5, 12.1, 13.1, 12.7 and 13.3 nm, respectively. For comparison, the RMS roughness of the P3HT:PCBM slow-grown film is 11.8 nm, which agrees with that reported in the literature.[11] The relative smoothness of the active layer is indicative of finer and more evenly distributed morphological features, which could reduce charge recombina-
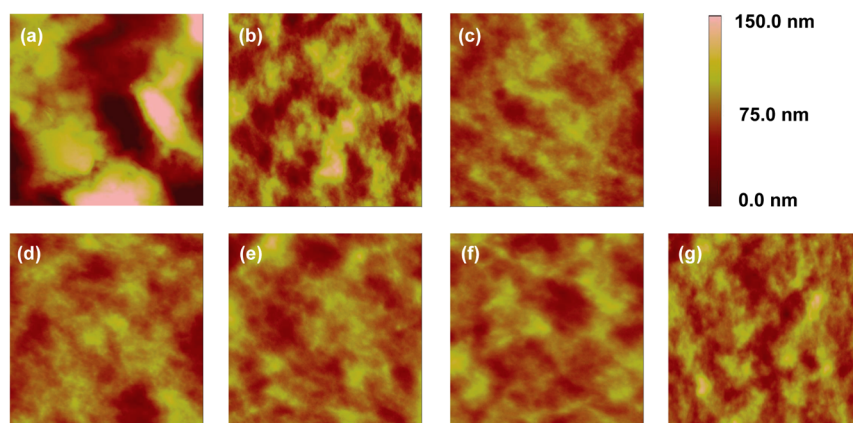
Figure 6. AFM height images (5 μm × 5 μm) of (a) P3HT:C1-NCBA, (b) P3HT:C2-NCBA, (c) P3HT:C3-NCBA, (d) P3HT:C4-NCBA, (e) P3HT:C5-NCBA, (f) P3HT:C6-NCBA, and (g) P3HT:PCBM blend films.
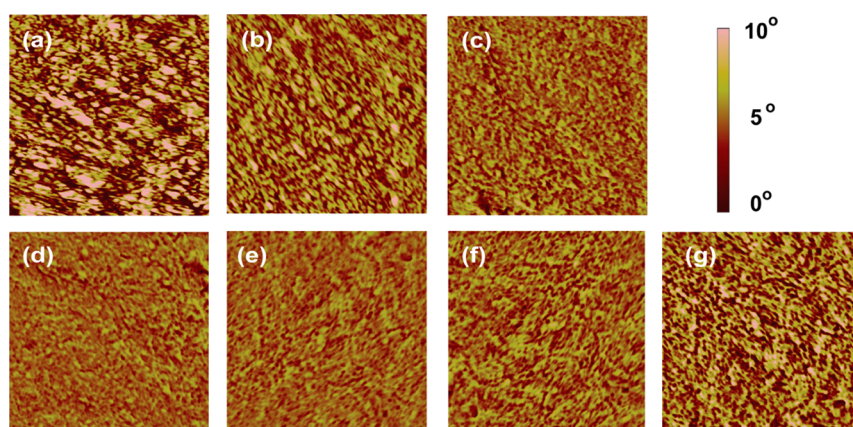
Figure 7. AFM phase images (1 μm × 1 μm) of (a) P3HT:C1-NCBA, (b) P3HT:C2-NCBA, (c) P3HT:C3-NCBA, (d) P3HT:C4-NCBA, (e) P3HT:C5-NCBA, (f) P3HT:C6-NCBA, and (g) P3HT:PCBM blend films.

tion. The largest RMS roughness of 33.6 nm was observed for the P3HT:C1-NCBA blend film, which may be ascribed to the poor miscibility of P3HT:C1-NCBA. In addition, it can be seen clearly from the AFM phase images that the P3HT:C1-NCBA blend film exhibits large phase separation with relatively big domain size. The large phase separation leads to a smaller donor:acceptor interfacial area, which is not favorable for efficient exciton dissociation, accounting for the low PCE of the P3HT:C1-NCBA PSCs.

Contact Angle. A previous study has already investigated the effects of the solubilizing group in the fullerene derivative on the interfacial interaction regarding P3HT and the photovoltaic performance.[40] They found that the difference of the photovoltaic performance is mainly due to the phase separation between P3HT and fullerene derivatives, which is caused by changes in the hydrophobicity of the fullerene derivatives and their interaction with P3HT. To further investigate the phase separation, we measured the contact angles (CAs) of two different solvents (water and glycerol) on Cn-NCBA and P3HT films (see Table 2 and Figure S1 in the Supporting Information). The water and glycerol CA of Cn-NCBA increased with the increase of alkoxy chain length, suggesting a corresponding increase in hydrophobicity. The surface tensions of Cn-NCBA and P3HT can be calculated from contact angle data[40,41] and are also summarized in Table 2. The surface tensions of Cn-NCBA decreased as the alkoxy chain length increased. To gain direct information about the

Table 2. Contact Angle Data of Cn-NCBA and P3HT Films

	water CA (deg)	glycerol CA (deg)	surface tension (mN m^{-1})	interfacial tension (mN m^{-1})
C1-NCBA	74.1	68.4	34.5	11.2
C2-NCBA	80.9	75.0	30.2	8.8
C3-NCBA	89.3	80.5	26.2	4.4
C4-NCBA	96.7	84.6	24.1	1.1
C5-NCBA	103.4	91.6	20.9	0.2
C6-NCBA	104.6	92.5	20.6	0.1
P3HT	106.3	93.7	20.3	

miscibility of Cn-NCBA and P3HT, the interfacial tension (γ) values between P3HT and Cn-NCBA were calculated using the following equation:[42]

$$\gamma_{12} = \gamma_1 + \gamma_2 - \frac{4\gamma_1^d\gamma_2^d}{\gamma_1^d + \gamma_2^d} - \frac{4\gamma_1^p\gamma_2^p}{\gamma_1^p + \gamma_2^p}$$

where γ_{12} is the interfacial tension between P3HT (1) and Cn-NCBA (2); γ_i is the surface tension of material i (i = 1 or 2); and γ_i^d and γ_i^p are the dispersion and polar components of γ_i, calculated from the contact angle with water and glycerol.

As shown in Table 2, the interfacial tension (γ) values between P3HT and Cn-NCBA decreased as the alkoxy chain length increased. Two materials with a low γ value could minimize the required energy penalty to produce a relatively well-mixed donor:acceptor blend with a large interfacial area,

5971

dx.doi.org/10.1021/am301629d | ACS Appl. Mater. Interfaces 2012, 4, 5966–5973

which facilitates efficient exciton diffusion and charge transfer. In contrast, the interfacial tension of C1-NCBA in blend with P3HT is much higher than those of others, leading to a poor miscibility of P3HT:C1-NCBA. The P3HT:C1-NCBA blend should have a large phase separation with smaller interfacial area, which was confirmed by atomic force microscopy (AFM) measurements, accounting for the low PCE of the P3HT:C1-NCBA PSCs.

CONCLUSIONS

In this paper, a series of alkoxy-substituted dihydronaphthyl-based [60]fullerene bisadduct derivatives, C*n*-NCBA (*n* = 1−6), were synthesized to investigate how the alkoxy chain length affected the photovoltaic properties of fullerene materials. Although C*n*-NCBA (*n* = 1−6) exhibit similar light absorption and electrochemical properties, polymer solar cells (PSCs) based on P3HT:C*n*-NCBA showed different photovoltaic properties. The preferable device is based on the blend of P3HT:C3-NCBA, demonstrating a PCE value of ca. 4.1%. While those with shorter or longer alkoxy-substituted dihydronaphthyl-based [60]fullerene bisadduct derivatives showed relatively lower power-conversion efficiency (PCE), C5-NCBA and C6-NCBA, with longer alkoxy chain length, showed relatively low electron mobilities, leading to relatively poor photovoltaic performance. A distinct phase separation for the P3HT:C1-NCBA blend film due to the large interfacial tension and poor miscibility with P3HT could be one reason for the low PCE of the C1-NCBA-based devices, which was supported by atomic force microscopy (AFM) and contact angle (CA) measurements. C3-NCBA may provide the most appropriate combination of electron mobility and miscibility with P3HT to achieve optimal photovoltaic properties. In a word, alkoxy chain length does have a pronounced effect on electron mobility, morphology, and, therefore, overall device performance. To further improve the device performance of the P3HT-based PSC, it is important to synthesize the fullerene bisadduct acceptor with appropriate carbon chain length that has high electron mobility and good miscibility with the donor simultaneously.

ASSOCIATED CONTENT

ⓢ Supporting Information

Electrochemical properties, MALDI-TOF MS, ^{1}H NMR and ^{13}C NMR spectra of C*n*-NCBA, contact angle data, SCLC measurements, absorption and photoluminescence spectra for P3HT:C*n*-NCBA and P3HT:PCBM blend films, and solar cells data. This information is available free of charge via the Internet at http://pubs.acs.org/.

AUTHOR INFORMATION

Corresponding Author

*E-mail: crwang@iccas.ac.cn (C.W.), tanzhanao@ncepu.edu.cn (Z.T.).

Notes

The authors declare no competing financial interest.

ACKNOWLEDGMENTS

REFERENCES

(1) Gunes, S.; Neugebauer, H.; Sariciftci, N. S. *Chem. Rev.* **2007**, *107*, 1324−1338.
(2) Thompson, B. C.; Frechet, J. M. J. *Angew. Chem., Int. Ed.* **2008**, *47*, 58−77.
(3) Dennler, G.; Scharber, M. C.; Brabec, C. J. *Adv. Mater.* **2009**, *21*, 1323−1338.
(4) Yu, G.; Gao, J.; Hummelen, J. C.; Wudl, F.; Heeger, A. J. *Science* **1995**, *270*, 1789−1791.
(5) Cheng, Y.-J.; Yang, S.-H.; Hsu, C.-S. *Chem. Rev.* **2009**, *109*, 5868−5923.
(6) Chen, J.; Cao, Y. *Acc. Chem. Res.* **2009**, *42*, 1709−1718.
(7) Li, Y. F. *Acc. Chem. Res.* **2012**, *45*, 723−733.
(8) He, Y.; Li, Y. *Phys. Chem. Chem. Phys.* **2011**, *13*, 1970−1983.
(9) Li, C.-Z.; Yip, H.-L.; Jen, A. K. Y. *J. Mater. Chem.* **2012**, *22*, 4161−4277.
(10) Hummelen, J. C.; Knight, B. W.; Lepeq, F.; Wudl, F.; Yao, J.; Wilkins, C. L. *J. Org. Chem.* **1995**, *60*, 532−538.
(11) Li, G.; Shrotriya, V.; Huang, J.; Yao, Y.; Moriarty, T.; Emery, K.; Yang, Y. *Nat. Mater.* **2005**, *4*, 864−868.
(12) Ma, W.; Yang, C.; Gong, X.; Lee, K.; Heeger, A. J. *Adv. Funct. Mater.* **2005**, *15*, 1617−1622.
(13) Brabec, C. J.; Cravino, A.; Meissner, D.; Sariciftci, N. S.; Fromherz, T.; Rispens, M. T.; Sanchez, L.; Hummelen, J. C. *Adv. Funct. Mater.* **2001**, *11*, 374−380.
(14) Kang, H.; Cho, C.-H.; Cho, H.-H.; Kang, T. E.; Kim, H. J.; Kim, K.-H.; Yoon, S. C.; Kim, B. J. *ACS Appl. Mater. Interfaces* **2011**, *4*, 110−116.
(15) Ross, R. B.; Cardona, C. M.; Guldi, D. M.; Sankaranarayanan, S. G.; Reese, M. O.; Kopidakis, N.; Peet, J.; Walker, B.; Bazan, G. C.; Van Keuren, E.; Holloway, B. C.; Drees, M. *Nat. Mater.* **2009**, *8*, 208−212.
(16) He, Y. J.; Zhao, G. J.; Peng, B.; Li, Y. F. *Adv. Funct. Mater.* **2010**, *20*, 3383−3389.
(17) Kim, K.-H.; Kang, H.; Nam, S. Y.; Jung, J.; Kim, P. S.; Cho, C.-H.; Lee, C.; Yoon, S. C.; Kim, B. J. *Chem. Mater.* **2011**, *23*, 5090−5095.
(18) He, Y.; Peng, B.; Zhao, G.; Zou, Y.; Li, Y. *J. Phys. Chem. C* **2011**, *115*, 4340−4344.
(19) Li, C.-Z.; Chien, S.-C.; Yip, H.-L.; Chueh, C.-C.; Chen, F.-C.; Matsuo, Y.; Nakamura, E.; Jen, A. K. Y. *Chem. Commun.* **2011**, *47*, 10082−10084.
(20) Voroshazi, E.; Vasseur, K.; Aernouts, T.; Heremans, P.; Baumann, A.; Deibel, C.; Xue, X.; Herring, A. J.; Athans, A. J.; Lada, T. A.; Richter, H.; Rand, B. P. *J. Mater. Chem.* **2011**, *21*, 17345−17352.
(21) Lenes, M.; Wetzelaer, G.; Kooistra, F. B.; Veenstra, S. C.; Hummelen, J. C.; Blom, P. W. M. *Adv. Mater.* **2008**, *20*, 2116−2119.
(22) Lenes, M.; Shelton, S. W.; Sieval, A. B.; Kronholm, D. F.; Hummelen, J. C.; Blom, P. W. M. *Adv. Funct. Mater.* **2009**, *19*, 3002−3007.
(23) He, Y. J.; Chen, H. Y.; Hou, J. H.; Li, Y. F. *J. Am. Chem. Soc.* **2010**, *132*, 1377−1382.
(24) Zhao, G. J.; He, Y. J.; Li, Y. F. *Adv. Mater.* **2010**, *22*, 4355−4358.
(25) Cheng, Y.-J.; Liao, M.-H.; Chang, C.-Y.; Kao, W.-S.; Wu, C.-E.; Hsu, C.-S. *Chem. Mater.* **2011**, *23*, 4056−4062.
(26) Meng, X. Y.; Zhang, W. Q.; Tan, Z. A.; Du, C.; Li, C. H.; Bo, Z. S.; Li, Y. F.; Yang, X. L.; Zhen, M. M.; Jiang, F.; Zheng, J. P.; Wang, T. S.; Jiang, L.; Shu, C. Y.; Wang, C. R. *Chem. Commun.* **2012**, *48*, 425−428.
(27) Meng, X. Y.; Zhang, W. Q.; Tan, Z. A.; Li, Y. F.; Ma, Y. H.; Wang, T. S.; Jiang, L.; Shu, C. Y.; Wang, C. R. *Adv. Funct. Mater.* **2012**, *22*, 2187−2193.
(28) Zhang, C.; Chen, S.; Xiao, Z.; Zuo, Q.; Ding, L. *Org. Lett.* **2012**, *14*, 1508−1511.
(29) Liu, C.; Xiao, S.; Shu, X.; Li, Y.; Xu, L.; Liu, T.; Yu, Y.; Zhang, L.; Liu, H.; Li, Y. *ACS Appl. Mater. Interfaces* **2012**, *4*, 1065−1071.
(30) Yelamaggad, C. V.; Achalkumar, A. S.; Rao, D. S. S.; Prasad, S. K. *J. Org. Chem.* **2007**, *72*, 8308−8318.
(31) Van der Made, A. W.; Van der Made, R. H. *J. Org. Chem.* **1993**, *58*, 1262−1263.

5972

dx.doi.org/10.1021/am301629d | *ACS Appl. Mater. Interfaces* 2012, 4, 5966−5973

(32) Nakamura, Y.; Asami, A.; Ogawa, T.; Inokuma, S.; Nishimura, J. *J. Am. Chem. Soc.* **2002**, *124*, 4329−4335.

(33) Hoey, M. D.; Dittmer, D. C. *J. Org. Chem.* **1991**, *56*, 1947−1948.

(34) Segura, J. L.; Martín, N. *Chem. Rev.* **1999**, *99*, 3199−3246.

(35) Zhao, G.; He, Y.; Xu, Z.; Hou, J.; Zhang, M.; Min, J.; Chen, H.-Y.; Ye, M.; Hong, Z.; Yang, Y.; Li, Y. *Adv. Funct. Mater.* **2010**, *20*, 1480−1487.

(36) Kooistra, F. B.; Knol, J.; Kastenberg, F.; Popescu, L. M.; Verhees, W. J. H.; Kroon, J. M.; Hummelen, J. C. *Org. Lett.* **2007**, *9*, 551−554.

(37) Varotto, A.; Treat, N. D.; Jo, J.; Shuttle, C. G.; Batara, N. A.; Brunetti, F. G.; Seo, J. H.; Chabinyc, M. L.; Hawker, C. J.; Heeger, A. J.; Wudl, F. *Angew. Chem., Int. Ed.* **2011**, *50*, 5166−5169.

(38) Mihailetchi, V. D.; Xie, H. X.; de Boer, B.; Koster, L. J. A.; Blom, P. W. M. *Adv. Funct. Mater.* **2006**, *16*, 699−708.

(39) MacKenzie, R. C. I.; Frost, J. M.; Nelson, J. *J. Chem. Phys.* **2010**, *132*, 064904.

(40) Kim, K.-H.; Kang, H.; Kim, H. J.; Kim, P. S.; Yoon, S. C.; Kim, B. J. *Chem. Mater.* **2012**, *24*, 2373−2381.

(41) Comyn, J. *Int. J. Adhes. Adhes.* **1992**, *12*, 145−149.

(42) Wu, S. *J. Polym. Sci., Part C: Polym. Symp.* **1971**, *34*, 19−30.